Histone H3K9 Methyltransferase G9a in Oocytes Is Essential for Preimplantation Development but Dispensable for CG Methylation Protection

Wan Kin Au Yeung, Julie Brind'Amour, Yu Hatano, Kazuo Yamagata, Robert Feil, Matthew Lorincz, Makoto Tachibana, Yoichi Shinkai, Hiroyuki Sasaki

Article

Cell Reports

Histone H3K9 Methyltransferase G9a in Oocytes Is Essential for Preimplantation Development but Dispensable for CG Methylation Protection

Graphical Abstract

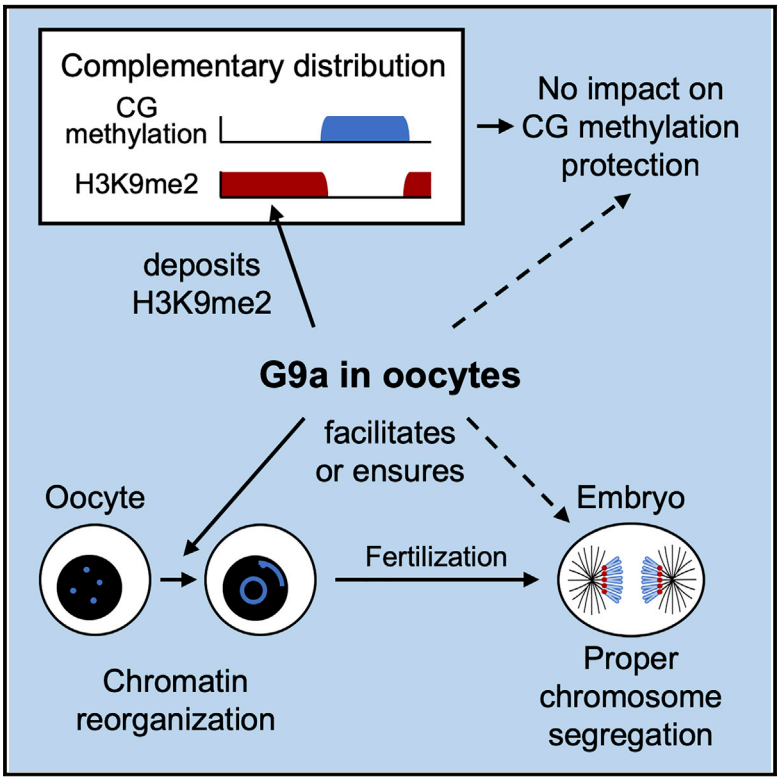

Highlights

- CG methylation and H3K9me2 are spatially separated in the genome of oocytes
- H3K9 methyltransferase G9a regulates chromatin reorganization in mouse oocytes
- Maternal G9a is vital for proper chromosome segregation in preimplantation embryos
- Maternal G9a has no impact on CG methylation protection in preimplantation embryos

Authors

Wan Kin Au Yeung, Julie Brind'Amour, Yu Hatano, ..., Makoto Tachibana, Yoichi Shinkai, Hiroyuki Sasaki

Correspondence

hsasaki@bioreg.kyushu-u.ac.jp

In Brief

Au Yeung et al. report that H3K9 methyltransferase G9a in mouse oocytes is essential for preimplantation development. Contrary to the previous model, however, maternal G9a is dispensable for CG methylation protection in zygotes and is instead important for chromatin reorganization in oocytes and proper chromosome segregation in preimplantation embryos.

Au Yeung et al., 2019, Cell Reports *27*, 282–293
April 2, 2019
https://doi.org/10.1016/j.celrep.2019.03.002

CellPress

OPEN ACCESS
CellPress

Cell Reports
Article

Histone H3K9 Methyltransferase G9a in Oocytes Is Essential for Preimplantation Development but Dispensable for CG Methylation Protection

Wan Kin Au Yeung,[1] Julie Brind'Amour,[2] Yu Hatano,[3] Kazuo Yamagata,[3] Robert Feil,[4] Matthew C. Lorincz,[2] Makoto Tachibana,[5] Yoichi Shinkai,[6] and Hiroyuki Sasaki[1,7,*]

[1]Division of Epigenomics and Development, Medical Institute of Bioregulation, Kyushu University, Fukuoka 812-8582, Japan
[2]Department of Medical Genetics, Life Sciences Institute, The University of British Columbia, Vancouver, BC V6T 1Z3, Canada
[3]Faculty of Biology-Oriented Science and Technology, KINDAI University, Wakayama 649-6493, Japan
[4]Institute of Molecular Genetics of Montpellier, CNRS, University of Montpellier, 34293 Montpellier, France
[5]Laboratory of Epigenome Dynamics, Graduate School of Frontier Biosciences, Osaka University, Osaka 565-0871, Japan
[6]Cellular Memory Laboratory, Cluster for Pioneering Research, RIKEN, Wako, Saitama 351-0198, Japan
[7]Lead Contact
*Correspondence: hsasaki@bioreg.kyushu-u.ac.jp
https://doi.org/10.1016/j.celrep.2019.03.002

SUMMARY

Mammalian histone methyltransferase G9a (also called EHMT2) deposits H3K9me2 on chromatin and is essential for postimplantation development. However, its role in oogenesis and preimplantation development remains poorly understood. We show that H3K9me2-enriched chromatin domains in mouse oocytes are generally depleted of CG methylation, contrasting with their association in embryonic stem and somatic cells. Oocyte-specific disruption of *G9a* results in reduced H3K9me2 enrichment and impaired reorganization of heterochromatin in oocytes, but only a modest reduction in CG methylation is detected. Furthermore, in both oocytes and 2-cell embryos, G9a depletion has limited impact on the expression of genes and retrotransposons. Although their CG methylation is minimally affected, preimplantation embryos derived from such oocytes show abnormal chromosome segregation and frequent developmental arrest. Our findings illuminate the functional importance of G9a independent of CG methylation in preimplantation development and call into question the proposed role for H3K9me2 in CG methylation protection in zygotes.

INTRODUCTION

G9a (also known as EHMT2) is a mammalian histone methyltransferase that mediates dimethylation of lysine 9 of core histone H3 (H3K9me2) with its catalytic SET domain (Tachibana et al., 2001, 2002; Collins et al., 2005). The protein forms a heterodimer with a structurally related G9a-like protein (GLP, also known as EHMT1), whose SET domain also mediates H3K9me2 deposition on chromatin (Tachibana et al., 2002, 2005). G9a is stabilized by dimerization with GLP (Tachibana et al., 2005). In mouse embryonic stem cells (ESCs) and primary somatic tissues, such as liver and brain, H3K9me2-enriched chromatin domains (up to 5 Mb) have been identified (Wen et al., 2009). Within such domains, a negative correlation between H3K9me2 deposition and gene expression is observed (Wen et al., 2009). These domains are highly conserved between human and mouse and often overlap with nuclear lamina-associated domains (LADs) (Wen et al., 2009; Kind et al., 2013).

G9a and GLP are essential for normal development, because their respective conventional knockout (KO) mice show postimplantation lethality before embryonic day 9.5 (E9.5) (Tachibana et al., 2002, 2005; Wagschal et al., 2008; Zylicz et al., 2015). Further studies showed that in addition to the loss of H3K9me2, global and local reductions in CG methylation, respectively, occur in *G9a* KO ESCs and postimplantation embryos (Ikegami et al., 2007; Dong et al., 2008; Tachibana et al., 2008; Leung et al., 2011; Myant et al., 2011; Auclair et al., 2016; Zhang et al., 2016). The genomic regions that show reduced CG methylation in KO ESCs and embryos include imprinting control regions (ICRs) and promoters of germline and developmental genes. Consistent with a role for G9a in CG methylation regulation, this protein is reported to interact with DNMT3A and DNMT3B (*de novo* DNA methyltransferases) via its ankyrin repeat domain (Epsztejn-Litman et al., 2008). The catalytic activity of the SET domain seems dispensable for CG methylation maintenance at the ICRs, intracisternal A particle (IAP) long terminal repeat (LTR) elements (belonging to class II endogenous retrovirus with lysine [K] tRNA primers [ERVKs]), and G9a target genes *Mage-a2* and *Wfdc15a* in ESCs (Dong et al., 2008; Tachibana et al., 2008; Zhang et al., 2016). The global reduction of CG methylation in *G9a* KO ESCs and its local reduction in *G9a* KO embryos are accompanied by upregulation of the *Mage-a2* gene, as well as class III murine endogenous retrovirus with leucine (L) tRNA primers (ERVLs, hereafter called MERVLs) and their chimeric transcripts (Tachibana et al., 2008; Leung et al., 2011; Maksakova et al., 2013; Zylicz et al., 2015; Auclair et al., 2016). In addition, G9a was reported to promote CG methylation maintenance in HeLa cells and ESCs by methylating DNA ligase LIG1 at lysine 126 (Ferry et al., 2017), which in

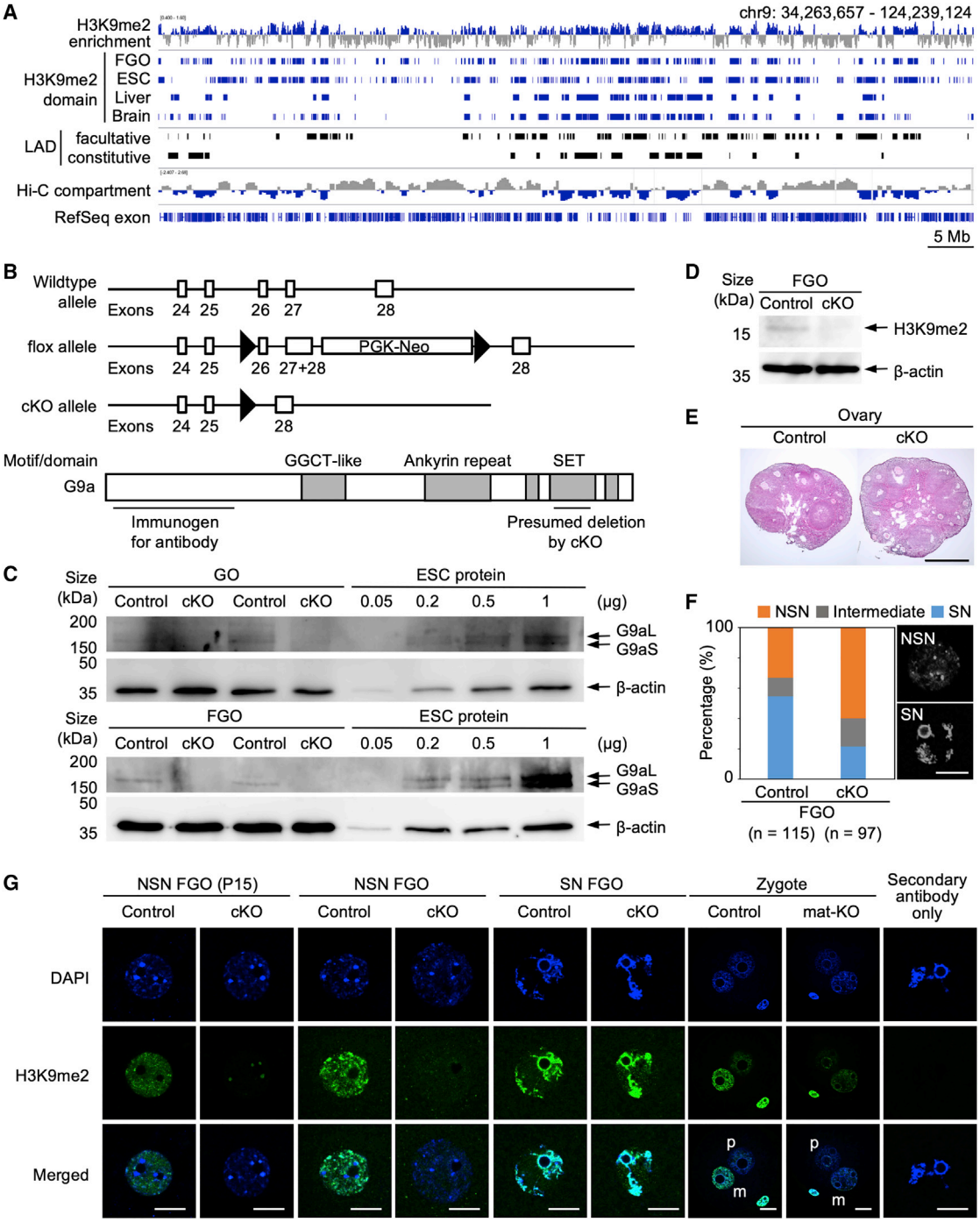

Figure 1. H3K9me2-Enriched Domains, *G9a* cKO, and Chromatin Reorganization in Mouse Oocytes

(A) H3K9me2 enrichment in FGOs plotted along a portion of mouse chromosome 9 (10-kb windows with 5-kb sliding steps). H3K9me2-enriched domains in FGOs (this study); ESCs, liver, and brain (Wen et al., 2009); facultative and constitutive LADs (fLADs and cLADs) (Peric-Hupkes et al., 2010; Meuleman et al., 2013); and Hi-C chromatin compartments of SN-type FGOs (Flyamer et al., 2017) are also shown. RefSeq exons are shown at the bottom.

(B) Wild-type and engineered *G9a* alleles and the domain architecture of G9a. A Cre-mediated recombination results in an in-frame deletion within the catalytic SET domain. GGCT, gamma-glutamyl cyclotransferase.

(C) Western blotting for G9a. GOs were collected at P10 and FGOs were collected 4 weeks after birth. The short isoform of G9a (G9aS) was predominant in GOs and FGOs, and the band was lost upon cKO. β-actin is a loading control.

(D) Western blotting for H3K9me2. FGOs were collected from adult ovaries (10–11 weeks). β-actin is a loading control.

(E) H&E staining of ovaries of 10–11 weeks. Scale bar, 500 μm.

(legend continued on next page)

turn recruits hemimethylated-CG binding factor UHRF1 and maintenance methyltransferase DNMT1 to replication sites. Thus, G9a is involved in CG methylation regulation via multiple pathways.

In postnatal ovaries, growing oocytes (GOs) progressively accumulate H3K9me2 (Kageyama et al., 2007), concomitant with the gain in CG and non-CG methylation (Smallwood et al., 2011; Kobayashi et al., 2012; Shirane et al., 2013). After fertilization, zygotes show an asymmetric H3K9me2 pattern, with high H3K9me2 in the maternal pronucleus and low H3K9me2 in the paternal pronucleus, and then the paternal genome progressively gains H3K9me2 from the late zygote to the cleavage stage (Liu et al., 2004; Santos et al., 2005; Ma et al., 2015). G9a, but not GLP, is responsible for this progressive gain in H3K9me2 (Ma et al., 2015). Thus, G9a and H3K9me2 are implicated in oogenesis and preimplantation development. Conditional KO (cKO) of *G9a* in primordial germ cells using *Tnap*-Cre results in reduced female fertility (Tachibana et al., 2007). However, the role of G9a produced during oocyte development is poorly understood.

Here, using *Zp3*-Cre driven oocyte-specific cKO, we examined the role of G9a in mouse oocytes and preimplantation embryos. Zylicz et al. (2018) adopted a similar approach to deplete maternal G9a and revealed a disrupted gene regulatory network at the 8-cell stage and destabilization of inner cell mass (ICM) lineages by the late blastocyst stage. However, our study reveals an earlier phenotype: impaired heterochromatin reorganization in oocytes, abnormal chromosome segregation in cleavage stage embryos, and limited CG methylation reduction essentially in gene-poor genomic regions in both oocytes and embryos. Our findings shed light on the functional importance of H3K9me2 in cleavage stage embryos and suggest the need for revisiting the proposed role for H3K9me2 in protection of the maternal genome from active CG demethylation.

RESULTS

G9a Expression and H3K9me2-Enriched Chromatin Domains in Oocytes

A previous RT-PCR study revealed upregulation of *G9a* during mouse oocyte growth (Kageyama et al., 2007). We reprocessed published RNA sequencing (RNA-seq) data from wild-type oocytes (Veselovska et al., 2015) and found that it is expressed at low levels in early GOs and progressively upregulated in late GOs and fully grown oocytes (FGOs) (Figure S1A).

It has been reported that GOs progressively accumulate H3K9me2 (Kageyama et al., 2007). Because various mouse cell types have large H3K9me2-enriched chromatin domains (Wen et al., 2009), we examined whether such domains are present in FGOs by ultra-low-input chromatin immunoprecipitation sequencing (ChIP-seq) (Brind'Amour et al., 2015) (Table S1). We identified 6,084 H3K9me2-enriched domains, varying in size from 20 kb to 1.35 Mb (with the median of 90 kb) and occupying 27.7% of the mouse genome (Figure 1A). These domains showed significant overlap with those identified in other cells or tissues (63.2%) (Wen et al., 2009; Filion and van Steensel, 2010), facultative or constitutive LADs (71.3%) (Peric-Hupkes et al., 2010; Meuleman et al., 2013), and the heterochromatic B compartments of FGOs (62.8%) identified by high-resolution chromosome conformation capture (Hi-C) (Flyamer et al., 2017) (Figure 1A).

Reduced H3K9me2 and Impaired Chromatin Reorganization in *G9a* cKO Oocytes

To investigate the role of G9a in oocytes and preimplantation embryos, we used mice carrying a floxed allele of *G9a* (Figure 1B) (Tachibana et al., 2007). We tested *Zp3*-Cre and *Gdf9*-Cre transgenes to delete exons 26 and 27 of *G9a* in GOs (de Vries et al., 2000; Lan et al., 2004). The cKO was designed to generate an 86-amino acid deletion and a single-amino acid insertion in the SET domain. Because the two Cre transgenes gave an identical phenotype, we used *Zp3*-Cre for further analyses. We refer to the materials obtained from [$G9a^{flox/flox}$, *Zp3*-Cre] females as cKO and those from $G9a^{flox/flox}$ females as control. By genotyping and RT-PCR, we confirmed that the Cre-mediated deletion was complete before postnatal day (P) 10 (Figures S1B and S1C). Western blotting showed depletion of G9a, presumably due to reduced protein stability, in both GOs and FGOs (Figure 1C). In addition, a significant loss of H3K9me2 was observed by western blotting in FGOs as expected (Figure 1D).

No discernible defect was observed in folliculogenesis in cKO ovaries (Figure 1E), and comparable numbers of FGOs were harvested from cKO and control ovaries (Figure S1D). Normal FGOs undergo heterochromatin reorganization, and two types of FGOs have been recognized: FGOs of surrounded nucleolus (SN) type have condensed chromatin surrounding the nucleolus, and those of non-surrounded nucleolus (NSN) type have less condensed chromatin (Bonnet-Garnier et al., 2012) (Figure S1E). Although NSN-type FGOs are transcriptionally active, SN-type FGOs are globally silent and developmentally more competent (Zuccotti et al., 1998; Bouniol-Baly et al., 1999; Liu and Aoki, 2002). Adult cKO ovaries had a reduced proportion of SN-type FGOs (21.6%, compared to 54.8% in control ovaries) and an increased proportion of NSN-type FGOs ($p < 5 \times 10^{-10}$, chi-square test) (Figure 1F). Thus, cKO oocytes have a defect in chromatin reorganization in FGOs.

Immunostaining for H3K9me2 revealed a dramatic decrease of this signal (~80%) in NSN-type cKO FGOs (Figures 1G and S1F), with only dotted signals remaining in DAPI-dense regions, especially at P15. A modest loss of H3K9me2 was observed in SN-type FGOs, especially in the heterochromatin around the

(F) Proportions of NSN-type and SN-type FGOs determined based on DAPI staining. Three batches (at least 28 FGOs each) were examined for each genotype. Representative DAPI images are also shown. Scale bar, 20 μm.

(G) Immunostaining of FGOs and zygotes for H3K9me2. FGOs were collected from P15 ovaries and adult ovaries (10–11 weeks), and zygotes were collected at 8 h. They were fixed, incubated with an anti-H3K9me2 antibody (green), and counterstained with DAPI (blue). Maternal (m) and paternal (p) pronuclei were distinguished based on size and position relative to the polar body. Two batches (at least 10 FGOs and zygotes) were examined for each stage and each genotype. Scale bar, 20 μm.

See also Figure S1 and Table S1.

nucleolus (see Discussion). In zygotes derived from cKO oocytes (maternal allele [mat]-KO zygotes), a significant reduction (~60%) of H3K9me2 was observed at 8 h post-fertilization in the female pronucleus (Figures 1G and S1F). In contrast, immunostaining revealed no change in histone H3 lysine 9 monomethylation (H3K9me1) or histone H3 lysine 9 trimethylation (H3K9me3) in either NSN-type or SN-type cKO FGOs (Figure S1G). Thus, the absence of G9a resulted in a significant, albeit incomplete, loss of H3K9me2 signal.

Developmental Defects of mat-KO Preimplantation Embryos

It was previously reported that *G9a* disruption in primordial germ cells results in a severe reduction of fertility in females (Tachibana et al., 2007). Upon natural crossing with wild-type males, our cKO females showed reduced fertility (probability of bearing live pups 60%, compared to 90% in control females) (Figure 2A) and a reduced litter size (2.8 pups, compared to 8.1 pups). Furthermore, they showed an increased rate of whole-litter mortality before weaning (66.7%, compared to 11.1%) (Figure 2A), with only 8 mat-KO pups (in two litters from ten plugged females) surviving to the adult stage (Figure S2A).

Upon *in vitro* fertilization (IVF) and culture, we frequently observed mat-KO embryos undergoing asymmetric cell division, cell fragmentation, and/or degeneration after the 2-cell stage (Figure S2B). Consequently, fewer mat-KO embryos developed to mid- and late blastocysts at 96 h (13.5%, compared to 64.5% in control embryos) and 120 h (32.4%, compared to 83.9%), respectively (Figures 2B and S2B). In addition, mat-KO blastocysts had a lower total number of cells (35.2, compared to 84.6 in control embryos) and fewer SOX17-positive primitive endoderm cells (2.5%, compared to 11.0%) (Figure S2C), consistent with the report by Zylicz et al. (2018). Because the reductions in litter size and blastocyst formation rate were similar to each other, embryos that survive the preimplantation period seem to have a high chance of being born.

To investigate the phenotype further, we performed live-cell imaging by injecting zygotes with mRNAs encoding α-tubulin fused with EGFP (cytoplasmic marker), together with those encoding histone H2B fused with mCherry (nuclear marker) (Figure 2C; Videos S1 and S2). Although mat-KO embryos looked normal until the 2-cell stage (Figures 2B and S2B), the first cell division was significantly delayed (Figure 2D). When blastocysts and retarded embryos identified at 102 h were traced back, the future blastocysts showed earlier progression to the 2-cell stage (Figure 2D). Closer investigation of the images revealed a higher frequency (50.0%, compared to 15.8%) of misaligned chromosomes and abnormal segregation, often manifested as lagging chromosomes and micronuclei, in mat-KO embryos had already occurred at the first cell division ($p < 1 \times 10^{-20}$, chi-square test) (Figure 2E).

Limited Reduction in CG and Non-CG Methylation in cKO Oocytes

Previous studies showed that DNA methylation is globally and locally disrupted in G9a-deficient ESCs and postimplantation embryos, respectively (Ikegami et al., 2007; Dong et al., 2008; Tachibana et al., 2008; Myant et al., 2011; Auclair et al., 2016; Zhang et al., 2016). To examine whether G9a has a role in DNA methylation in oocytes, we performed whole-genome bisulfite sequencing (WGBS) (Miura et al., 2012). The high reproducibility of our WGBS data was confirmed in biological replicates (R = 0.80 to ~0.99 at 500-kb windows) (Table S2) and by comparison with the published data (R = 0.99) (Shirane et al., 2013).

The global methylation levels examined at CG and non-CG sites in control GOs (P10), FGOs (adult), and metaphase II (MII) oocytes (Figure 3A; Table S2) were consistent with the ongoing *de novo* methylation during oocyte growth and maturation (Smallwood et al., 2011; Kobayashi et al., 2012; Shirane et al., 2013). Surprisingly, most H3K9me2-enriched domains had low levels of CG methylation in FGOs (Figures 3B and 3C), which is in clear contrast to the findings in ESCs and somatic cells, in which H3K9me2-enriched regions are highly CG methylated (Figure S3A) (data from Wen et al., 2009, reprocessed). Furthermore, the global CG methylation level was only slightly lower in cKO FGOs and MII oocytes relative to control oocytes (39.2% versus 41.5% in FGOs and 43.6% versus 45.2% in MII oocytes) (Table S2). The non-CG methylation showed a greater reduction in cKO FGOs (from 3.4% to 2.7%) and MII oocytes (from 4.6% to 3.3%) (Table S2), and this 20%–30% reduction was uniform across the genome (Figure 3D). Thus, depletion of G9a had a limited but differential impact on *de novo* CG and non-CG methylation during oocyte growth.

We next investigated whether CG methylation is affected in genomic regions previously identified as G9a targets in KO ESCs and postimplantation embryos. Consistent with the global analysis, most targets in ESCs (423/441 = 95.9%) (Tachibana et al., 2008; Auclair et al., 2016) and embryos (636/686 = 92.7%) (Auclair et al., 2016) (Figure S3B) showed no or little methylation loss (<20%) in cKO FGOs. It was previously reported that G9a is important for CG methylation maintenance at ICRs in ESCs (Dong et al., 2008; Zhang et al., 2016). All 13 maternally methylated ICRs are located outside of H3K9me2-enriched domains (Figure S3C) and showed no or minimal (12.2% at most) reduction in CG methylation in cKO FGOs (Figure 3E). The *Gnas1A* and *Mest* ICRs, which showed the greatest reduction, were previously shown to be modestly affected in *Uhrf1* cKO FGOs (Maenohara et al., 2017). Furthermore, the *Slc38a4* ICR, which is known to be affected in *G9a* KO postimplantation embryos (Auclair et al., 2016), showed a normal methylation level in cKO FGOs. Similarly, while it is known that almost all ERVs and only ERVL elements show reduced methylation in KO ESCs and embryos, respectively (Auclair et al., 2016), ERVs showed little change (<20%) in cKO FGOs, with only two exceptions (RLTR13D4 and RLTR46A2, which are ERVKs) (Figure S3D). Altogether, these results reveal that the contribution of G9a to CG methylation regulation in oocytes is modest.

G9a Is Dispensable for Protection against CG Demethylation in Preimplantation Embryos

It has been proposed that H3K9me2 deposited in oocytes promotes the recruitment of Stella (also called Dppa3 or Pgc7) to maternal chromatin in zygotes and that this protein, in turn, protects CG methylation from Tet3-mediated hydroxylation and subsequent demethylation (Nakamura et al., 2007, 2012). However, a report suggested an opposite role for Stella (prevention

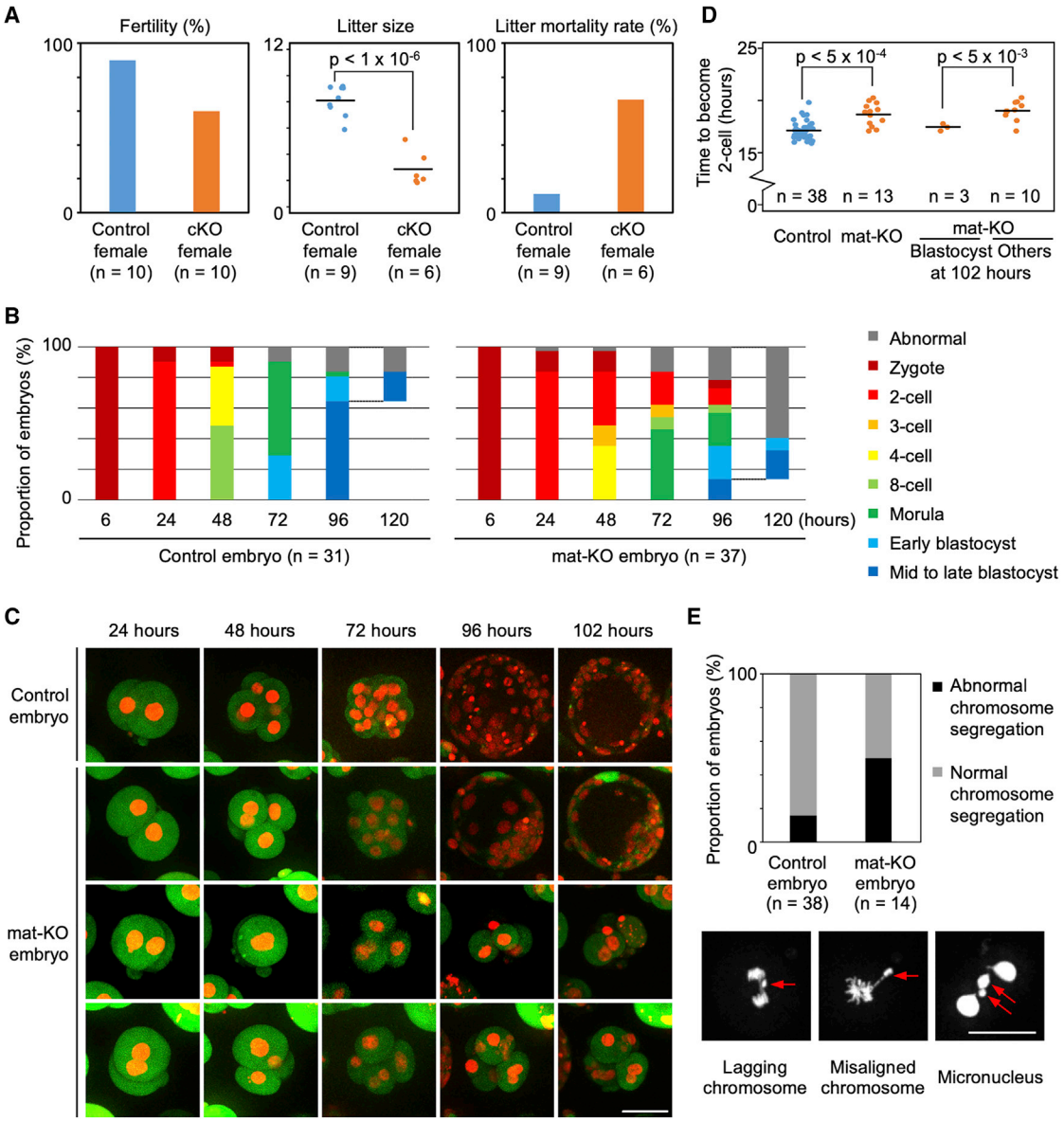

Figure 2. Developmental Defects in mat-KO Preimplantation Embryos

(A) Fertility (successful breeding), litter size, and whole-litter mortality rate before weaning. Horizontal bars in litter size show the mean values. The p value was determined by t test.

(B) Developmental stages of IVF embryos assessed at indicated time points. Mid- to late blastocysts were removed at 96 h, and only retarded embryos were allowed to develop for an additional 24 h and assessed at 120 h.

(C) Snapshots of IVF embryos observed under live-cell imaging. H2B-mCherry (red) and EGFP-α-tubulin (green) are the markers for chromatin and cytoplasm, respectively. Thirty-eight control and 14 mat-KO embryos were examined. Scale bar, 50 μm.

(D) Time to become a 2-cell embryo. The mat-KO embryos were divided into blastocysts and retarded embryos at 102 h and traced back to determine the timing of the first cell division. Horizontal bars show the mean values. The p value was determined by t test.

(E) Proportions of embryos showing abnormal chromosome segregation during zygote to 2-cell transition. Representative images are shown. Arrows (red) indicate the respective abnormalities. Scale bar, 50 μm.

See also Figure S2 and Videos S1 and S2.

of *de novo* CG methylation) in oocytes (Li et al., 2018). To assess the impact of *G9a* cKO on CG methylation and demethylation in preimplantation embryos, we performed WGBS on mat-KO early 2-cell embryos and mid- to late blastocysts (Table S2). For 2-cell embryos, we crossed cKO females with JF1 males so that the parental alleles could be distinguished using strain-specific single-nucleotide polymorphisms (SNPs) (Takada et al., 2013). Furthermore, to avoid the confounding influence of DNA replication, only early 2-cell embryos, harvested within 2 h of the first mitotic division, were subjected to WGBS. To match the

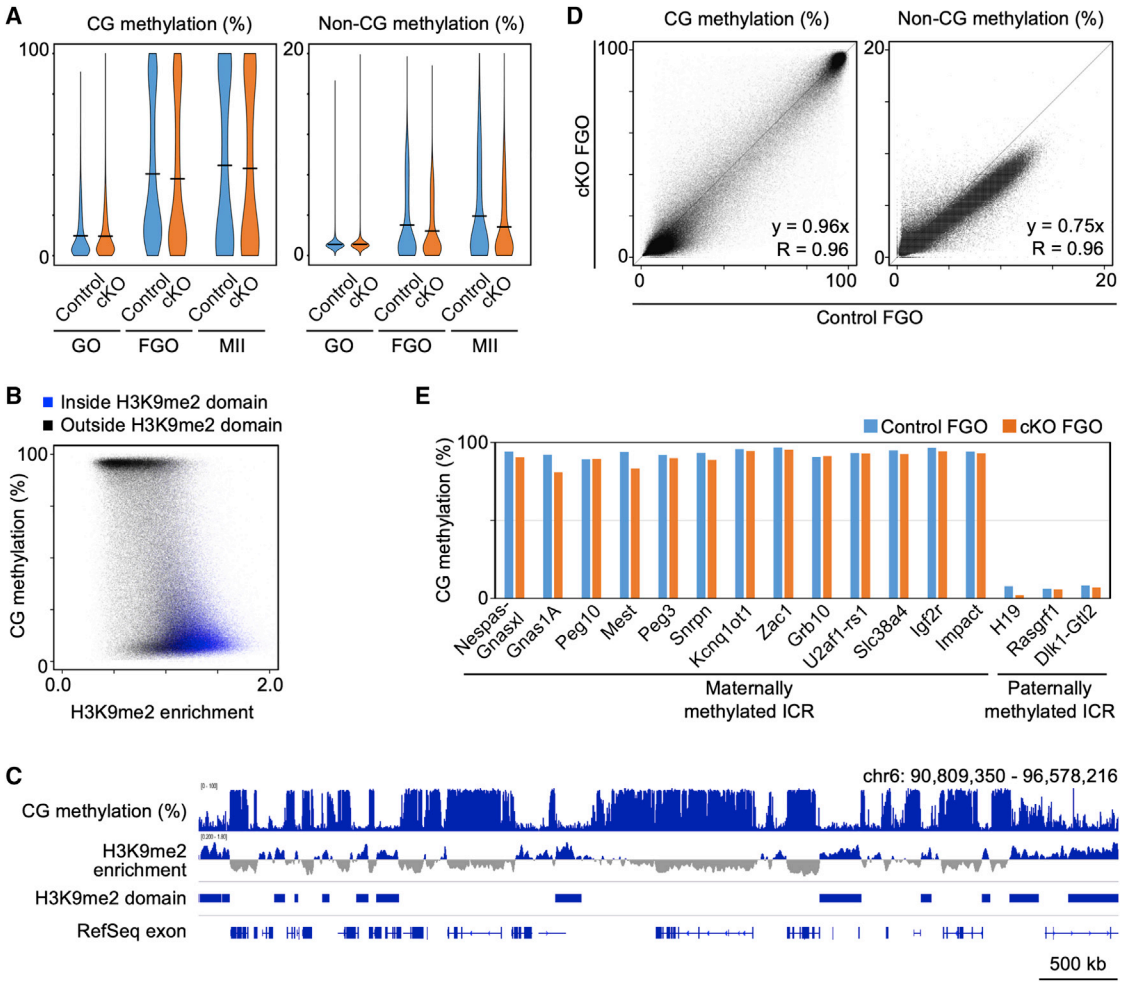

Figure 3. Limited Reduction in CG and Non-CG Methylation in cKO FGOs

(A) Violin plots showing distributions of regional CG or non-CG methylation levels (10-kb windows) in GOs, FGOs, and MII oocytes. Black bars indicate the mean values. These values are different from the global methylation levels.

(B) Scatterplot comparing regional CG methylation levels and H3K9me2 enrichment in wild-type FGOs (10-kb windows). Blue dots indicate genomic windows inside H3K9me2-enriched domains.

(C) CG methylation profile of a portion of mouse chromosome 6 (10-kb windows with 5-kb sliding steps). H3K9me2 enrichment is also shown. H3K9me2-enriched domains and RefSeq exons are indicated at the bottom.

(D) Scatterplots comparing regional CG or non-CG methylation levels (10-kb windows) of control and cKO FGOs. Pearson product-moment correlation coefficients and slopes of linear regression are indicated.

(E) CG methylation levels at the ICRs in FGOs.

See also Figure S3 and Tables S1 and S2.

developmental stage, only early 2-cell mat-KO embryos morphologically similar to the control embryos were collected.

During the progression from 2-cell embryos to blastocysts, the level of global CG methylation decreased from 46.7% to 15.0% in control embryos (Table S2), consistent with ongoing global demethylation. Strikingly, the methylation levels of mat-KO 2-cell embryos and blastocysts (43.4% and 14.6%, respectively) were only slightly lower than those of control embryos (46.7% and 15.0%) (Table S2). Using SNPs, the lower level of CG methylation observed in mat-KO 2-cell embryos was attributed to the maternal genome (35.7%, compared to 42.2% in control embryos), with no decrease in the paternal genome (55.2%, compared to 53.9%) (Figure 4A; Table S2). A greater but still modest reduction in CG methylation was observed in mat-KO 2-cell embryos (42.2–35.7 = 6.5% reduction in the maternal genome) compared to cKO MII oocytes (4.6–3.3 = 1.6% reduction) (Table S2), indicating that G9a plays a minor role in DNA methylation homeostasis after fertilization.

Although this observation seems consistent with the proposed role for H3K9me2 in protection against CG demethylation (Nakamura et al., 2007, 2012), most informative G9a targets previously identified in ESCs and postimplantation embryos (262/314 = 83.4% and 129/168 = 76.8%, respectively) (Tachibana et al., 2008; Auclair et al., 2016) showed little CG methylation loss

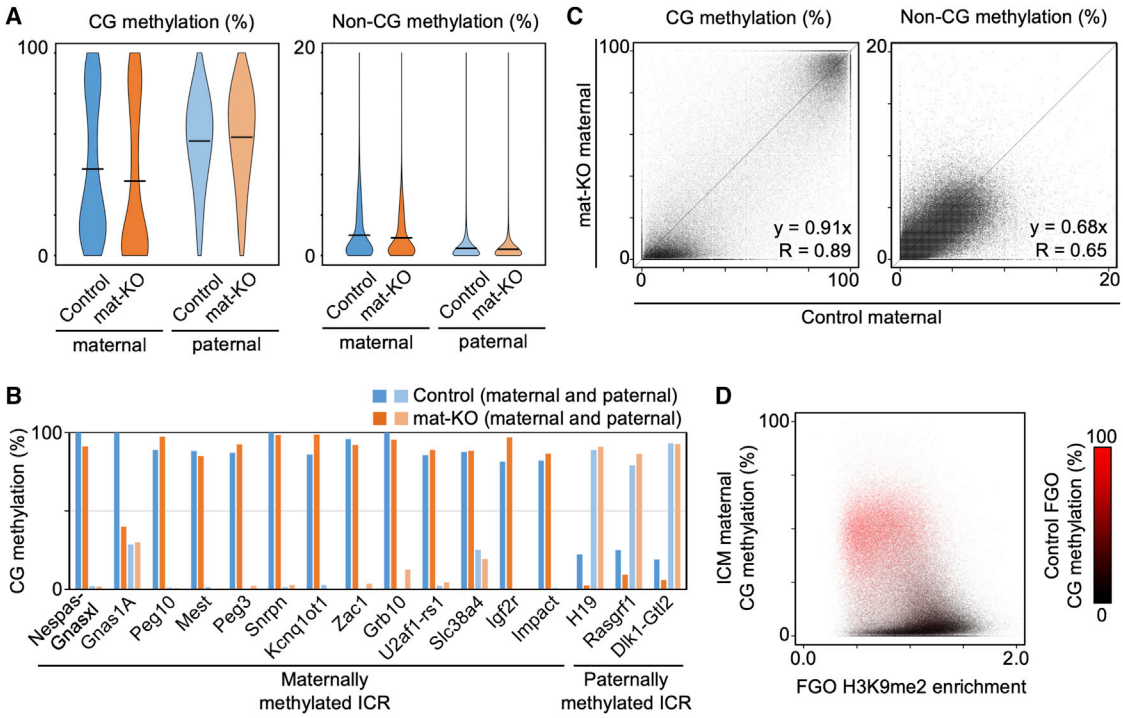

Figure 4. G9a Is Dispensable for Protection against CG Demethylation in Preimplantation Embryos

(A) Violin plots showing distributions of regional CG or non-CG methylation levels (10-kb windows) in control and mat-KO 2-cell embryos. Black bars indicate the mean values. These values are different from the global methylation levels.

(B) CG methylation levels at the ICRs in control and mat-KO 2-cell embryos.

(C) Scatterplots comparing regional CG or non-CG methylation levels (10-kb windows) of the maternal genomes from control and mat-KO 2-cell embryos. Pearson product-moment correlation coefficients and slopes of linear regression are indicated.

(D) Scatterplot comparing regional CG methylation levels in the maternal genome of the ICM (Wang et al., 2014) and H3K9me2 enrichment in wild-type FGOs (10-kb windows). The color gradient shows the CG methylation levels in control FGOs.

See also Figure S4 and Tables S1 and S2.

(<20%) in the maternal genome of mat-KO 2-cell embryos (Figure S4A). Similarly, with only a few exceptions (the three ERVKs RLTR13D1, RLTR46A2, and RLTR20A3 and the non-MERVL ERVL mouse transposon subfamily C [MTC]), ERVs also showed little change (<20%) in CG methylation (Figure S4B). Furthermore, most maternally methylated ICRs (11/12) and all three paternally methylated ICRs were essentially unaffected in mat-KO 2-cell embryos (Figure 4B). The *Peg10*, *Mest*, and *Peg3* ICRs and IAP elements, which were reported to be affected in *Stella* mat-KO embryos (Nakamura et al., 2007), showed little change in *G9a* mat-KO embryos. An exception was the significantly reduced methylation at the *Gnas1A* ICR ($p < 5 \times 10^{-11}$, chi-square test), which was also affected in cKO FGOs (Figure 3D). Thus, the reduction in H3K9me2 caused by *G9a* cKO did not induce general ICR demethylation, calling into question the proposed role for this histone modification in protection against CG demethylation (Nakamura et al., 2012).

The modest reduction in CG methylation of the maternal genome was largely attributable to regions that showed low levels of CG methylation in control embryos (Figure 4C), corresponding to the H3K9me2-enriched domains in FGOs (Figures 1A and 3B). Such regions showed a modest gain in CG methylation in control embryos soon after fertilization (before the 2-cell stage) (Figure S4C), which may be mediated by DNMT3A and DNMT1 (Amouroux et al., 2016). The reduced methylation in mat-KO embryos was partly attributable to the lack of such *de novo* methylation (Figure S4D). In addition, analysis of published allelic WGBS data from the ICM (Wang et al., 2014) showed that regions of the maternal genome with high levels of CG methylation correspond to those with relatively low levels of H3K9me2 in FGOs (Figure 4D). Altogether, these results show that although H3K9me2 has a modest role in regulating CG methylation in H3K9me2-enriched domains, this histone modification has no role in protecting highly methylated regions in the maternal genome against demethylation in preimplantation embryos.

Limited Changes in Expression of Genes and ERVs in cKO Oocytes and mat-KO Embryos

Analysis of published RNA-seq data reveals that the activation of zygotic *G9a* occurs after the mid-2-cell stage (Figure S5A) (Deng et al., 2014). To examine the impact of *G9a* cKO on transcription, we performed RNA-seq on cKO FGOs and mat-KO mid-2-cell embryos (24 h) (Table S1). Although zygotic genes of one subset are already active (biallelic transcripts) in mid-2-cell embryos, most are not (maternal transcripts only) (Flach et al., 1982; Matsumoto et al., 1994).

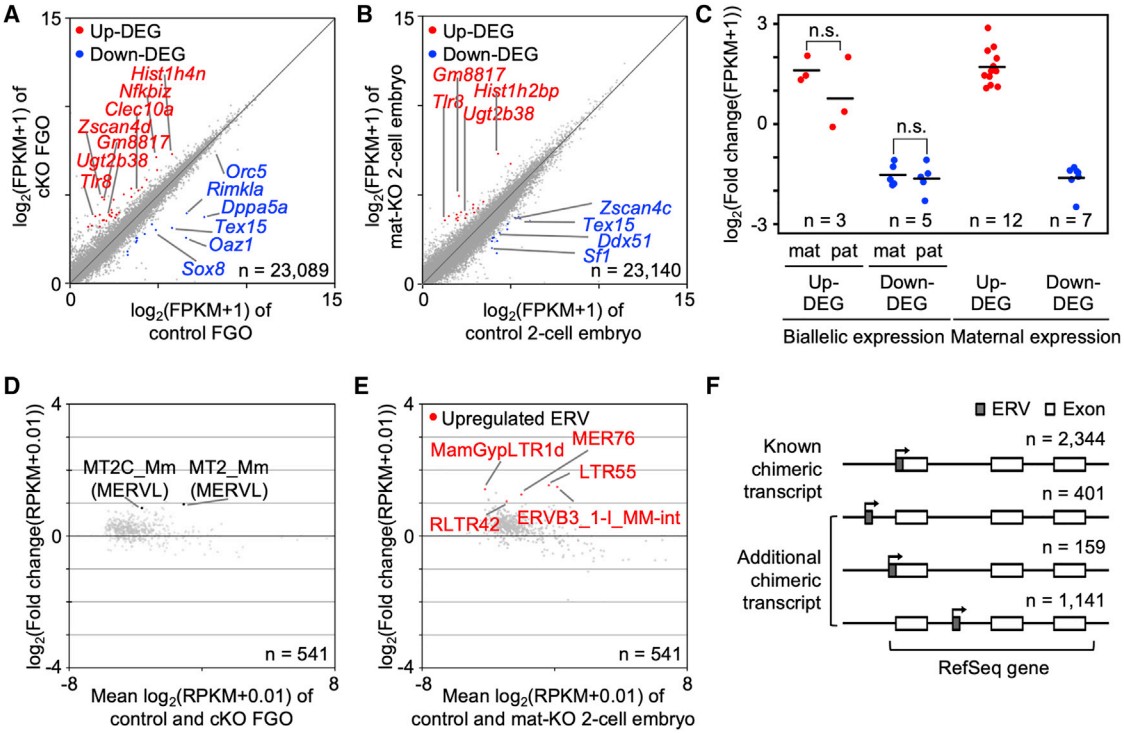

Figure 5. Limited Changes in Expression of Genes and ERVs in cKO FGOs and mat-KO Embryos

(A) Scatterplot comparing the gene expression profiles in control and cKO FGOs. The up-DEGs and down-DEGs are highlighted in red and blue, respectively.

(B) Scatterplot comparing the gene expression profiles in control and mat-KO 2-cell embryos. The up-DEGs and down-DEGs are highlighted in red and blue, respectively.

(C) Distributions of the expression fold changes of the DEGs. mat and pat indicate expression from the maternal and paternal allele, respectively. For the maternally expressed DEGs [mat/(mat + pat) ≥ 0.85], the expression fold change of the maternal transcripts is shown. Horizontal bars show the mean values. The p values were determined by t test. n.s., not significant.

(D) MA plot of the expression fold change of individual ERVs in FGOs. The x axis shows the mean expression level of each element in FGOs (control and cKO combined), and the y axis shows the fold change. No upregulated (≥2-fold) ERV was identified.

(E) MA plot of the expression fold change of individual ERVs in 2-cell embryos. The x axis shows the mean expression level of each element in 2-cell embryos (control and mat-KO combined), and the y axis shows the fold change. Upregulated ERVs (≥2-fold) are highlighted in red.

(F) Schematic representation of the ERV-RefSeq chimeric transcripts. A total number of transcripts identified in FGOs and 2-cell embryos is indicated for each category.

See also Figure S5 and Tables S1 and S3.

The impact of G9a depletion on RefSeq genes was limited in both FGOs and 2-cell embryos. We identified only 41 differentially expressed genes (DEGs, ≥2-fold difference) in FGOs, of which 28 were upregulated (up-DEGs) and 13 were downregulated (down-DEGs) (Figure 5A; Table S3). Expression of three up-DEGs and two down-DEGs was previously examined in SN-type and NSN-type FGOs (Ma et al., 2013), and based on the results, their altered expression in cKO FGOs was attributable to the reduced SN-type/NSN-type ratio (Figure 1E). The DEG showing the greatest upregulation was *Zscan4d* (8-fold) (Figures 5A and S5B), which is a member of the SCAN domain-containing zinc finger protein family important for developmental competence of germ cells, preimplantation embryos, and ESCs (Falco et al., 2007; Zalzman et al., 2010; Amano et al., 2013; Ishiguro et al., 2017). In mat-KO 2-cell embryos, we identified only 30 DEGs (17 up-DEGs and 13 down-DEGs) (Figure 5B; Table S3), of which 27 DEGs (15 up-DEGs and 12 down-DEGs) were informative for allelic analysis: while 8 DEGs (3 up-DEGs and 5 down-DEGs) showed biallelic expression, the remaining 19 DEGs (12 up-DEGs and 7 down-DEGs) showed maternal expression (proportion of maternal transcripts out of all informative transcripts ≥ 0.85) (Figure 5C). In all 8 biallelically expressed DEGs, both parental alleles were affected (Figure 5C). These results suggest that maternal G9a can act on the paternal genome, consistent with previous findings (Liu et al., 2004; Ma et al., 2015). Contrary to the upregulation of *Zscan4d* in cKO FGOs, a 3.6-fold downregulation of *Zscan4c* was observed in mat-KO embryos (Figures 5B and S5B). It remains to be investigated whether the misregulation of the *Zscan4* genes (Falco et al., 2007) and other development-related DEGs (Table S3) contributes to the phenotype.

Most DEGs identified in FGOs and 2-cell embryos were located outside of H3K9me2-enriched domains (38/41 = 92.7% and 27/30 = 90.0%, respectively), and only 18.4% (7/38, with 3 being non-informative) and 5.6% of them (1/18, with 12 being non-informative) showed a change in CG methylation (≥20%). The

changes were always found in gene bodies, with a positive correlation between methylation and expression (Table S3). Most G9a targets found in ESCs and postimplantation embryos (427/441 = 96.8% and 57/60 = 92.7%, respectively) (Tachibana et al., 2008; Auclair et al., 2016) were unaffected (<2-fold) in cKO FGOs and mat-KO embryos (Figure S5C).

ERVs also showed virtually no or only modest derepression in cKO FGOs and mat-KO 2-cell embryos (Figures 5D and 5E). While MT2 and MT2C, members of the ERVL family, are derepressed in *G9a* KO ESCs (Maksakova et al., 2013), their transcripts showed a less than 2-fold increase in cKO FGOs (Figure 5D). In mat-KO embryos, only five ERV families showed $\geq$2-fold derepression (MERVL not among them), and none showed $\geq$4-fold derepression (Figure 5E). Our results are consistent with the findings reported by Zylicz et al. (2018).

ERVs often provide alternative promoters to genes in oocytes (Macfarlan et al., 2012; Peaston et al., 2004; Veselovska et al., 2015). In addition to 2,344 RefSeq transcripts containing ERV at their 5′ ends, we identified 1,701 ERV-RefSeq chimeric transcripts expressed in FGOs, 2-cell embryos, or both (Figure 5F), including 5 cKO-specific and 2 mat-KO-specific ones. Thus, there were 2,845 and 3,425 chimeric transcripts in FGOs and 2-cell embryos, respectively (2,225 were common). Most of these transcripts were not affected by G9a depletion: only 180/2,845 transcripts (6.3%) and 246/3,425 transcripts (7.2%) were upregulated ($\geq$2-fold) in cKO FGOs and mat-KO embryos, respectively. Only 35 and 30 of the upregulated chimeric transcripts were driven by MERVL LTRs in FGOs and 2-cell embryos, respectively, and these transcripts contributed little to the DEGs. Furthermore, only 5/28 (17.9%) of the upregulated DEGs had a MERVL LTR at their 5′ ends in FGOs (Figure S5D); none were found in 2-cell embryos. Thus, unlike ESCs and postimplantation embryos, in which G9a plays an important role in MERVL repression (Tachibana et al., 2008; Leung et al., 2011; Maksakova et al., 2013; Zylicz et al., 2015), this histone methyltransferase is apparently dispensable for MERVL regulation in oocytes and preimplantation embryos.

DISCUSSION

We have revealed a role for G9a in H3K9me2 deposition and heterochromatin reorganization in mouse oocytes. Mouse FGOs had H3K9me2-enriched chromatin domains (Figure 1A), and depletion of G9a in GOs resulted in abnormal chromosome segregation, developmental delay, and frequent arrest of cleavage stage embryos (Figure 2). Together with the report that maternal depletion of G9a results in impaired ICM lineage segregation (Zylicz et al., 2018), our study establishes the importance of maternal G9a in preimplantation development. However, unlike in ESCs and postimplantation embryos, only limited changes were observed in CG methylation, gene regulation, or ERV repression upon G9a depletion in oocytes and preimplantation embryos (Figures 3, 4, and 5). G9a depletion resulted in a mild reduction in CG methylation only in gene-poor regions, corresponding to the H3K9me2-enriched domains, and almost no change in highly methylated transcribed regions, including most genes, ICRs, and ERVs (Figures 3 and 4). Thus, the role of G9a during oogenesis and preimplantation development is distinct from that observed during postimplantation development.

It has been proposed that H3K9me2 deposited in oocytes recruits Stella specifically to the maternal chromatin of zygotes to protect against Tet3-mediated hydroxylation and subsequent CG demethylation of the maternal genome (Nakamura et al., 2007, 2012). However, at the maternally methylated ICRs reported to be affected in *Stella* KO zygotes (Nakamura et al., 2007), *G9a* cKO in GOs resulted in no or only limited CG methylation loss (Figure 4B), despite significant loss of H3K9me2. H3K9me2 enrichment and CG methylation show mutually exclusive genomic distributions in FGOs (Figure 3B), making their functional association unlikely. Li et al. (2018) revisited the role of Stella in oocytes and zygotes and reported that contrary to previous reports, Stella suppresses aberrant *de novo* CG methylation. Altogether, we suggest that the role of H3K9me2 in CG methylation protection (Nakamura et al., 2012) should be reconsidered. Our results also suggest that despite the reported function of this enzyme in LIG1 methylation and subsequent UHRF1 recruitment, maternal G9a is dispensable for CG methylation maintenance in zygotes (Ferry et al., 2017).

We observed that *G9a* cKO GOs, FGOs, and zygotes show significant but partial H3K9me2 loss (Figures 1F and 1G). The dotted signals detected in P15 cKO FGOs and the more organized signals around the nucleolus in SN-type cKO FGOs are reminiscent of H3K9me3 enrichment over satellite repeat regions (Figures 1F and S1G). SUV39H1 and SUV39H2, which are responsible for H3K9me3 deposition in heterochromatin regions (Peters et al., 2003), could contribute to the H3K9me2 signals by creating a reaction intermediate. In *G9a* KO ESCs, H3K9me2-enriched domains are lost, and the peaks shift to overlap with H3K9me3-enriched regions, likely reflecting transient H3K9me2, the catalytic intermediate of SETDB1- (also known as ESET) or SUV39-deposited H3K9me3 in heterochromatin regions (Chen et al., 2018).

The precise cause for the developmental phenotype of mat-KO preimplantation embryos remains obscure. A study reported that a loss of maternal G9a disrupts the gene regulatory network in 8-cell embryos and destabilizes ICM lineages by the late blastocyst stage (Zylicz et al., 2018). We confirmed the skewed lineage differentiation (Figure S2C) but found an earlier phenotype: delayed progression to the 2-cell stage and presence of misaligned chromosomes and abnormal segregation already manifesting at the first division (Figure 2E). Because cKO FGOs and mat-KO 2-cell embryos showed only limited defects in gene expression and ERV repression (Figure 5), the alternation to the gene regulatory network is an unlikely cause for the developmental delay and partial lethality. Instead, apparently normal cKO FGOs already had a defect in heterochromatin reorganization (increased NSN-type and decreased SN-type FGOs) (Figure 1E), which is a hallmark of developmental competence (Zuccotti et al., 1998). Perhaps reduced deposition of H3K9me2 in G9a-target domains, which largely overlap with the LADs and heterochromatin compartments (Figure 1A), hampers the formation of condensed chromatin surrounding the nucleolus. However, the involvement of some DEGs in developmental phenotype may be worth further investigation.

In conclusion, our findings illuminate the functional importance of maternal G9a in early development and its distinct roles in preimplantation and postimplantation development. They also suggest the need for revisiting the proposed role for H3K9me2 in protection of the maternal genome against active CG demethylation. Whether alternative histone modifications play a role in this process remains to be determined, but those that show a positive correlation with regions methylated in oocytes, such as H3K36me3 (Stewart et al., 2015; Brind'Amour et al., 2018), are worthy of further investigation.

STAR★METHODS

Detailed methods are provided in the online version of this paper and include the following:

- KEY RESOURCES TABLE
- CONTACT FOR REAGENT AND RESOURCE SHARING
- EXPERIMENTAL MODEL AND SUBJECT DETAILS
  - Animal Work
  - Genetically Modified Mice and Genotyping
- METHOD DETAILS
  - Fertility Testing
  - Oocyte Collection, IVF and Embryo Culture
  - RT-PCR
  - Western Blotting
  - Ovary Sectioning and Hematoxylin-Eosin Staining
  - Immunostaining
  - WGBS, RNA-seq, and ChIP-seq
  - Microinjection and Live-cell Imaging
- QUANTIFICATION AND STATISTICAL ANALYSIS
  - Reference Sequences
  - WGBS Data Analysis
  - RNA-seq Data Analysis
  - ChIP-seq Data Analysis
  - Hi-C Data Analysis
  - Statistical Analysis and Graph Generation
- DATA AND SOFTWARE AVAILABILITY

SUPPLEMENTAL INFORMATION

Supplemental Information can be found with this article online at https://doi.org/10.1016/j.celrep.2019.03.002.

ACKNOWLEDGMENTS

We thank T. Ishiuchi, M. Unoki, H. Toh, J. Oishi, K. Toriyama, T. Akinaga, M. Miyake, M. Tanaka (Kyushu University), J. Richard Albert (University of British Columbia), A. Yamada (RIKEN), and H. Miyachi (Kyoto University) for their assistance. This work was supported in part by JSPS KAKENHI grants to H.S. (JP25112010 and JP18H05214) and K.Y. (JP25116005), a Canadian Institutes of Health Research grant to M.C.L. (MOP-133417), and funding from Genome British Columbia to M.C.L. (SOF154).

AUTHOR CONTRIBUTIONS

W.K.A.Y., J.B., and Y.H. conducted the experiments and analyzed the data. W.K.A.Y., M.C.L., K.Y., R.F., M.T., Y.S., and H.S. conceived the project, designed the experiments, analyzed the data, and wrote the manuscript. M.T. and Y.S. produced the animal strain.

DECLARATION OF INTERESTS

The authors declare no competing interests.

Received: May 30, 2018
Revised: January 7, 2019
Accepted: February 27, 2019
Published: April 2, 2019

REFERENCES

Amano, T., Hirata, T., Falco, G., Monti, M., Sharova, L.V., Amano, M., Sheer, S., Hoang, H.G., Piao, Y., Stagg, C.A., et al. (2013). Zscan4 restores the developmental potency of embryonic stem cells. Nat. Commun. *4*, 1966.

Amouroux, R., Nashun, B., Shirane, K., Nakagawa, S., Hill, P.W.S., D'Souza, Z., Nakayama, M., Matsuda, M., Turp, A., Ndjetehe, E., et al. (2016). *De novo* DNA methylation drives 5hmC accumulation in mouse zygotes. Nat. Cell Biol. *18*, 225–233.

Auclair, G., Borgel, J., Sanz, L.A., Vallet, J., Guibert, S., Dumas, M., Cavelier, P., Girardot, M., Forné, T., Feil, R., and Weber, M. (2016). EHMT2 directs DNA methylation for efficient gene silencing in mouse embryos. Genome Res. *26*, 192–202.

Bao, W., Kojima, K.K., and Kohany, O. (2015). Repbase Update, a database of repetitive elements in eukaryotic genomes. Mob. DNA *6*, 11.

Bonnet-Garnier, A., Feuerstein, P., Chebrout, M., Fleurot, R., Jan, H.U., Debey, P., and Beaujean, N. (2012). Genome organization and epigenetic marks in mouse germinal vesicle oocytes. Int. J. Dev. Biol. *56*, 877–887.

Bouniol-Baly, C., Hamraoui, L., Guibert, J., Beaujean, N., Szöllösi, M.S., and Debey, P. (1999). Differential transcriptional activity associated with chromatin configuration in fully grown mouse germinal vesicle oocytes. Biol. Reprod. *60*, 580–587.

Brind'Amour, J., Liu, S., Hudson, M., Chen, C., Karimi, M.M., and Lorincz, M.C. (2015). An ultra-low-input native ChIP-seq protocol for genome-wide profiling of rare cell populations. Nat. Commun. *6*, 6033.

Brind'Amour, J., Kobayashi, H., Richard Albert, J., Shirane, K., Sakashita, A., Kamio, A., Bogutz, A., Koike, T., Karimi, M.M., Lefebvre, L., et al. (2018). LTR retrotransposons transcribed in oocytes drive species-specific and heritable changes in DNA methylation. Nat. Commun. *9*, 3331.

Chen, C.C.L., Goyal, P., Karimi, M.M., Abildgaard, M.H., Kimura, H., and Lorincz, M.C. (2018). H3S10ph broadly marks early-replicating domains in interphase ESCs and shows reciprocal antagonism with H3K9me2. Genome Res. *28*, 37–51.

Collins, R.E., Tachibana, M., Tamaru, H., Smith, K.M., Jia, D., Zhang, X., Selker, E.U., Shinkai, Y., and Cheng, X. (2005). *In vitro* and *in vivo* analyses of a Phe/Tyr switch controlling product specificity of histone lysine methyltransferases. J. Biol. Chem. *280*, 5563–5570.

de Vries, W.N., Binns, L.T., Fancher, K.S., Dean, J., Moore, R., Kemler, R., and Knowles, B.B. (2000). Expression of Cre recombinase in mouse oocytes: a means to study maternal effect genes. Genesis *26*, 110–112.

Deng, Q., Ramsköld, D., Reinius, B., and Sandberg, R. (2014). Single-cell RNA-seq reveals dynamic, random monoallelic gene expression in mammalian cells. Science *343*, 193–196.

Dong, K.B., Maksakova, I.A., Mohn, F., Leung, D., Appanah, R., Lee, S., Yang, H.W., Lam, L.L., Mager, D.L., Schübeler, D., et al. (2008). DNA methylation in ES cells requires the lysine methyltransferase G9a but not its catalytic activity. EMBO J. *27*, 2691–2701.

Epsztejn-Litman, S., Feldman, N., Abu-Remaileh, M., Shufaro, Y., Gerson, A., Ueda, J., Deplus, R., Fuks, F., Shinkai, Y., Cedar, H., and Bergman, Y. (2008). *De novo* DNA methylation promoted by G9a prevents reprogramming of embryonically silenced genes. Nat. Struct. Mol. Biol. *15*, 1176–1183.

Falco, G., Lee, S.L., Stanghellini, I., Bassey, U.C., Hamatani, T., and Ko, M.S.H. (2007). Zscan4: a novel gene expressed exclusively in late 2-cell embryos and embryonic stem cells. Dev. Biol. *307*, 539–550.

Ferry, L., Fournier, A., Tsusaka, T., Adelmant, G., Shimazu, T., Matano, S., Kirsh, O., Amouroux, R., Dohmae, N., Suzuki, T., et al. (2017). Methylation of DNA Ligase 1 by G9a/GLP recruits UHRF1 to replicating DNA and regulates DNA methylation. Mol. Cell *67*, 550–565.

Filion, G.J., and van Steensel, B. (2010). Reassessing the abundance of H3K9me2 chromatin domains in embryonic stem cells. Nat. Genet. *42*, 4, author reply 5–6.

Flach, G., Johnson, M.H., Braude, P.R., Taylor, R.A., and Bolton, V.N. (1982). The transition from maternal to embryonic control in the 2-cell mouse embryo. EMBO J. *1*, 681–686.

Flyamer, I.M., Gassler, J., Imakaev, M., Brandão, H.B., Ulianov, S.V., Abdennur, N., Razin, S.V., Mirny, L.A., and Tachibana-Konwalski, K. (2017). Single-nucleus Hi-C reveals unique chromatin reorganization at oocyte-to-zygote transition. Nature *544*, 110–114.

Habibi, E., Brinkman, A.B., Arand, J., Kroeze, L.I., Kerstens, H.H.D., Matarese, F., Lepikhov, K., Gut, M., Brun-Heath, I., Hubner, N.C., et al. (2013). Whole-genome bisulfite sequencing of two distinct interconvertible DNA methylomes of mouse embryonic stem cells. Cell Stem Cell *13*, 360–369.

Heinz, S., Benner, C., Spann, N., Bertolino, E., Lin, Y.C., Laslo, P., Cheng, J.X., Murre, C., Singh, H., and Glass, C.K. (2010). Simple combinations of lineage-determining transcription factors prime cis-regulatory elements required for macrophage and B cell identities. Mol. Cell *38*, 576–589.

Ho, Y., Wigglesworth, K., Eppig, J.J., and Schultz, R.M. (1995). Preimplantation development of mouse embryos in KSOM: augmentation by amino acids and analysis of gene expression. Mol. Reprod. Dev. *41*, 232–238.

Hon, G.C., Rajagopal, N., Shen, Y., McCleary, D.F., Yue, F., Dang, M.D., and Ren, B. (2013). Epigenetic memory at embryonic enhancers identified in DNA methylation maps from adult mouse tissues. Nat. Genet. *45*, 1198–1206.

Ikegami, K., Iwatani, M., Suzuki, M., Tachibana, M., Shinkai, Y., Tanaka, S., Greally, J.M., Yagi, S., Hattori, N., and Shiota, K. (2007). Genome-wide and locus-specific DNA hypomethylation in G9a deficient mouse embryonic stem cells. Genes Cells *12*, 1–11.

Ishiguro, K.I., Monti, M., Akiyama, T., Kimura, H., Chikazawa-Nohtomi, N., Sakota, M., Sato, S., Redi, C.A., Ko, S.B., and Ko, M.S. (2017). Zscan4 is expressed specifically during late meiotic prophase in both spermatogenesis and oogenesis. *In Vitro* Cell. Dev. Biol. Anim. *53*, 167–178.

Kageyama, S., Liu, H., Kaneko, N., Ooga, M., Nagata, M., and Aoki, F. (2007). Alterations in epigenetic modifications during oocyte growth in mice. Reproduction *133*, 85–94.

Karolchik, D., Barber, G.P., Casper, J., Clawson, H., Cline, M.S., Diekhans, M., Dreszer, T.R., Fujita, P.A., Guruvadoo, L., Haeussler, M., et al. (2014). The UCSC Genome Browser database: 2014 update. Nucleic Acids Res. *42*, D764–D770.

Kim, D., Langmead, B., and Salzberg, S.L. (2015). HISAT: a fast spliced aligner with low memory requirements. Nat. Methods *12*, 357–360.

Kind, J., Pagie, L., Ortabozkoyun, H., Boyle, S., de Vries, S.S., Janssen, H., Amendola, M., Nolen, L.D., Bickmore, W.A., and van Steensel, B. (2013). Single-cell dynamics of genome-nuclear lamina interactions. Cell *153*, 178–192.

Kobayashi, H., Sakurai, T., Imai, M., Takahashi, N., Fukuda, A., Yayoi, O., Sato, S., Nakabayashi, K., Hata, K., Sotomaru, Y., et al. (2012). Contribution of intragenic DNA methylation in mouse gametic DNA methylomes to establish oocyte-specific heritable marks. PLoS Genet. *8*, e1002440.

Krueger, F., and Andrews, S.R. (2011). Bismark: a flexible aligner and methylation caller for Bisulfite-Seq applications. Bioinformatics *27*, 1571–1572.

Lan, Z.J., Xu, X., and Cooney, A.J. (2004). Differential oocyte-specific expression of Cre recombinase activity in GDF-9-iCre, Zp3cre, and Msx2Cre transgenic mice. Biol. Reprod. *71*, 1469–1474.

Langmead, B., and Salzberg, S.L. (2012). Fast gapped-read alignment with Bowtie 2. Nat. Methods *9*, 357–359.

Leung, D.C., Dong, K.B., Maksakova, I.A., Goyal, P., Appanah, R., Lee, S., Tachibana, M., Shinkai, Y., Lehnertz, B., Mager, D.L., et al. (2011). Lysine methyltransferase G9a is required for *de novo* DNA methylation and the establishment, but not the maintenance, of proviral silencing. Proc. Natl. Acad. Sci. USA *108*, 5718–5723.

Lewis, B.C., Klimstra, D.S., Socci, N.D., Xu, S., Koutcher, J.A., and Varmus, H.E. (2005). The absence of p53 promotes metastasis in a novel somatic mouse model for hepatocellular carcinoma. Mol. Cell. Biol. *25*, 1228–1237.

Li, Y., Zhang, Z., Chen, J., Liu, W., Lai, W., Liu, B., Li, X., Liu, L., Xu, S., Dong, Q., et al. (2018). Stella safeguards the oocyte methylome by preventing *de novo* methylation mediated by DNMT1. Nature *564*, 136–140.

Liu, H., and Aoki, F. (2002). Transcriptional activity associated with meiotic competence in fully grown mouse GV oocytes. Zygote *10*, 327–332.

Liu, H., Kim, J.M., and Aoki, F. (2004). Regulation of histone H3 lysine 9 methylation in oocytes and early pre-implantation embryos. Development *131*, 2269–2280.

Ma, J.Y., Li, M., Luo, Y.B., Song, S., Tian, D., Yang, J., Zhang, B., Hou, Y., Schatten, H., Liu, Z., and Sun, Q.Y. (2013). Maternal factors required for oocyte developmental competence in mice: transcriptome analysis of non-surrounded nucleolus (NSN) and surrounded nucleolus (SN) oocytes. Cell Cycle *12*, 1928–1938.

Ma, X.S., Chao, S.B., Huang, X.J., Lin, F., Qin, L., Wang, X.G., Meng, T.G., Zhu, C.C., Schatten, H., Liu, H.L., and Sun, Q.Y. (2015). The dynamics and regulatory mechanism of pronuclear H3K9me2 asymmetry in mouse zygotes. Sci. Rep. *5*, 17924.

Macfarlan, T.S., Gifford, W.D., Driscoll, S., Lettieri, K., Rowe, H.M., Bonanomi, D., Firth, A., Singer, O., Trono, D., and Pfaff, S.L. (2012). Embryonic stem cell potency fluctuates with endogenous retrovirus activity. Nature *487*, 57–63.

Maenohara, S., Unoki, M., Toh, H., Ohishi, H., Sharif, J., Koseki, H., and Sasaki, H. (2017). Role of UHRF1 in *de novo* DNA methylation in oocytes and maintenance methylation in preimplantation embryos. PLoS Genet. *13*, e1007042.

Maksakova, I.A., Thompson, P.J., Goyal, P., Jones, S.J., Singh, P.B., Karimi, M.M., and Lorincz, M.C. (2013). Distinct roles of KAP1, HP1 and G9a/GLP in silencing of the two-cell-specific retrotransposon MERVL in mouse ES cells. Epigenetics Chromatin *6*, 15.

Matsumoto, K., Anzai, M., Nakagata, N., Takahashi, A., Takahashi, Y., and Miyata, K. (1994). Onset of paternal gene activation in early mouse embryos fertilized with transgenic mouse sperm. Mol. Reprod. Dev. *39*, 136–140.

Meuleman, W., Peric-Hupkes, D., Kind, J., Beaudry, J.B., Pagie, L., Kellis, M., Reinders, M., Wessels, L., and van Steensel, B. (2013). Constitutive nuclear lamina-genome interactions are highly conserved and associated with A/T-rich sequence. Genome Res. *23*, 270–280.

Miura, F., Enomoto, Y., Dairiki, R., and Ito, T. (2012). Amplification-free whole-genome bisulfite sequencing by post-bisulfite adaptor tagging. Nucleic Acids Res. *40*, e136.

Myant, K., Termanis, A., Sundaram, A.Y., Boe, T., Li, C., Merusi, C., Burrage, J., de Las Heras, J.I., and Stancheva, I. (2011). LSH and G9a/GLP complex are required for developmentally programmed DNA methylation. Genome Res. *21*, 83–94.

Nakamura, T., Arai, Y., Umehara, H., Masuhara, M., Kimura, T., Taniguchi, H., Sekimoto, T., Ikawa, M., Yoneda, Y., Okabe, M., et al. (2007). PGC7/Stella protects against DNA demethylation in early embryogenesis. Nat. Cell Biol. *9*, 64–71.

Nakamura, T., Liu, Y.J., Nakashima, H., Umehara, H., Inoue, K., Matoba, S., Tachibana, M., Ogura, A., Shinkai, Y., and Nakano, T. (2012). PGC7 binds histone H3K9me2 to protect against conversion of 5mC to 5hmC in early embryos. Nature *486*, 415–419.

Peaston, A.E., Evsikov, A.V., Graber, J.H., de Vries, W.N., Holbrook, A.E., Solter, D., and Knowles, B.B. (2004). Retrotransposons regulate host genes in mouse oocytes and preimplantation embryos. Dev. Cell *7*, 597–606.

Peric-Hupkes, D., Meuleman, W., Pagie, L., Bruggeman, S.W., Solovei, I., Brugman, W., Gräf, S., Flicek, P., Kerkhoven, R.M., van Lohuizen, M., et al. (2010). Molecular maps of the reorganization of genome-nuclear lamina interactions during differentiation. Mol. Cell *38*, 603–613.

Pertea, M., Pertea, G.M., Antonescu, C.M., Chang, T.C., Mendell, J.T., and Salzberg, S.L. (2015). StringTie enables improved reconstruction of a transcriptome from RNA-seq reads. Nat. Biotechnol. *33*, 290–295.

Pertea, M., Kim, D., Pertea, G.M., Leek, J.T., and Salzberg, S.L. (2016). Transcript-level expression analysis of RNA-seq experiments with HISAT, StringTie and Ballgown. Nat. Protoc *11*, 1650–1667.

Peters, A.H., Kubicek, S., Mechtler, K., O'Sullivan, R.J., Derijck, A.A.H.A., Perez-Burgos, L., Kohlmaier, A., Opravil, S., Tachibana, M., Shinkai, Y., et al. (2003). Partitioning and plasticity of repressive histone methylation states in mammalian chromatin. Mol. Cell *12*, 1577–1589.

Santos, F., Peters, A.H., Otte, A.P., Reik, W., and Dean, W. (2005). Dynamic chromatin modifications characterise the first cell cycle in mouse embryos. Dev. Biol. *280*, 225–236.

Schneider, C.A., Rasband, W.S., and Eliceiri, K.W. (2012). NIH Image to ImageJ: 25 years of image analysis. Nat. Methods *9*, 671–675.

Shirane, K., Toh, H., Kobayashi, H., Miura, F., Chiba, H., Ito, T., Kono, T., and Sasaki, H. (2013). Mouse oocyte methylomes at base resolution reveal genome-wide accumulation of non-CpG methylation and role of DNA methyltransferases. PLoS Genet. *9*, e1003439.

Smallwood, S.A., Tomizawa, S., Krueger, F., Ruf, N., Carli, N., Segonds-Pichon, A., Sato, S., Hata, K., Andrews, S.R., and Kelsey, G. (2011). Dynamic CpG island methylation landscape in oocytes and preimplantation embryos. Nat. Genet. *43*, 811–814.

Stewart, K.R., Veselovska, L., Kim, J., Huang, J., Saadeh, H., Tomizawa, S., Smallwood, S.A., Chen, T., and Kelsey, G. (2015). Dynamic changes in histone modifications precede *de novo* DNA methylation in oocytes. Genes Dev. *29*, 2449–2462.

Tachibana, M., Sugimoto, K., Fukushima, T., and Shinkai, Y. (2001). Set domain-containing protein, G9a, is a novel lysine-preferring mammalian histone methyltransferase with hyperactivity and specific selectivity to lysines 9 and 27 of histone H3. J. Biol. Chem. *276*, 25309–25317.

Tachibana, M., Sugimoto, K., Nozaki, M., Ueda, J., Ohta, T., Ohki, M., Fukuda, M., Takeda, N., Niida, H., Kato, H., and Shinkai, Y. (2002). G9a histone methyltransferase plays a dominant role in euchromatic histone H3 lysine 9 methylation and is essential for early embryogenesis. Genes Dev. *16*, 1779–1791.

Tachibana, M., Ueda, J., Fukuda, M., Takeda, N., Ohta, T., Iwanari, H., Sakihama, T., Kodama, T., Hamakubo, T., and Shinkai, Y. (2005). Histone methyltransferases G9a and GLP form heteromeric complexes and are both crucial for methylation of euchromatin at H3-K9. Genes Dev. *19*, 815–826.

Tachibana, M., Nozaki, M., Takeda, N., and Shinkai, Y. (2007). Functional dynamics of H3K9 methylation during meiotic prophase progression. EMBO J. *26*, 3346–3359.

Tachibana, M., Matsumura, Y., Fukuda, M., Kimura, H., and Shinkai, Y. (2008). G9a/GLP complexes independently mediate H3K9 and DNA methylation to silence transcription. EMBO J. *27*, 2681–2690.

Takada, T., Ebata, T., Noguchi, H., Keane, T.M., Adams, D.J., Narita, T., Shin-I, T., Fujisawa, H., Toyoda, A., Abe, K., et al. (2013). The ancestor of extant Japanese fancy mice contributed to the mosaic genomes of classical inbred strains. Genome Res. *23*, 1329–1338.

Toh, H., Shirane, K., Miura, F., Kubo, N., Ichiyanagi, K., Hayashi, K., Saitou, M., Suyama, M., Ito, T., and Sasaki, H. (2017). Software updates in the Illumina HiSeq platform affect whole-genome bisulfite sequencing. BMC Genomics *18*, 31.

Tomizawa, S., Kobayashi, H., Watanabe, T., Andrews, S., Hata, K., Kelsey, G., and Sasaki, H. (2011). Dynamic stage-specific changes in imprinted differentially methylated regions during early mammalian development and prevalence of non-CpG methylation in oocytes. Development *138*, 811–820.

Veselovska, L., Smallwood, S.A., Saadeh, H., Stewart, K.R., Krueger, F., Maupetit-Méhouas, S., Arnaud, P., Tomizawa, S., Andrews, S., and Kelsey, G. (2015). Deep sequencing and *de novo* assembly of the mouse oocyte transcriptome define the contribution of transcription to the DNA methylation landscape. Genome Biol. *16*, 209.

Wagschal, A., Sutherland, H.G., Woodfine, K., Henckel, A., Chebli, K., Schulz, R., Oakey, R.J., Bickmore, W.A., and Feil, R. (2008). G9a histone methyltransferase contributes to imprinting in the mouse placenta. Mol. Cell. Biol. *28*, 1104–1113.

Wang, L., Zhang, J., Duan, J., Gao, X., Zhu, W., Lu, X., Yang, L., Zhang, J., Li, G., Ci, W., et al. (2014). Programming and inheritance of parental DNA methylomes in mammals. Cell *157*, 979–991.

Wen, B., Wu, H., Shinkai, Y., Irizarry, R.A., and Feinberg, A.P. (2009). Large histone H3 lysine 9 dimethylated chromatin blocks distinguish differentiated from embryonic stem cells. Nat. Genet. *41*, 246–250.

Yamagata, K., and Ueda, J. (2013). Long-term live-cell imaging of mammalian preimplantation development and derivation process of pluripotent stem cells from the embryos. Dev. Growth Differ. *55*, 378–389.

Yamagata, K., Suetsugu, R., and Wakayama, T. (2009). Long-term, six-dimensional live-cell imaging for the mouse preimplantation embryo that does not affect full-term development. J. Reprod. Dev. *55*, 343–350.

Younesy, H., Möller, T., Lorincz, M.C., Karimi, M.M., and Jones, S.J.M. (2015). VisRseq: R-based visual framework for analysis of sequencing data. BMC Bioinformatics *16* (*Suppl 11*), S2.

Zalzman, M., Falco, G., Sharova, L.V., Nishiyama, A., Thomas, M., Lee, S.L., Stagg, C.A., Hoang, H.G., Yang, H.T., Indig, F.E., et al. (2010). Zscan4 regulates telomere elongation and genomic stability in ES cells. Nature *464*, 858–863.

Zhang, T., Termanis, A., Özkan, B., Bao, X.X., Culley, J., de Lima Alves, F., Rappsilber, J., Ramsahoye, B., and Stancheva, I. (2016). G9a/GLP complex maintains imprinted DNA methylation in embryonic stem cells. Cell Rep. *15*, 77–85.

Zuccotti, M., Giorgi Rossi, P., Martinez, A., Garagna, S., Forabosco, A., and Redi, C.A. (1998). Meiotic and developmental competence of mouse antral oocytes. Biol. Reprod. *58*, 700–704.

Zylicz, J.J., Dietmann, S., Günesdogan, U., Hackett, J.A., Cougot, D., Lee, C., and Surani, M.A. (2015). Chromatin dynamics and the role of G9a in gene regulation and enhancer silencing during early mouse development. eLife *4*, e09571.

Zylicz, J.J., Borensztein, M., Wong, F.C.K., Huang, Y., Lee, C., Dietmann, S., and Surani, M.A. (2018). G9a regulates temporal preimplantation developmental program and lineage segregation in blastocyst. eLife *7*, e33361.

STAR★METHODS

KEY RESOURCES TABLE

REAGENT or RESOURCE	SOURCE	IDENTIFIER
Antibodies		
Rabbit monoclonal anti-G9a antibody	abcam	Cat# ab185050; RRID: AB_2792982
Mouse monoclonal anti-β-actin	Santa Cruz	Cat# sc-69879; RRID: AB_1119529
Mouse monoclonal anti-H3K9me2 antibody	MBL	Cat# MABI0307; RRID: AB_11124951
Mouse monoclonal anti-H3K9me2 antibody	abcam	Cat# ab1220; RRID: AB_449854
Chemicals, Peptides, and Recombinant Proteins		
EmbryoMax KSOM Medium (1X) w/ 1/2 Amino Acids	Merck Millipore	MR-106-D
Critical Commercial Assays		
KAPA HiFi HotStart ReadyMix PCR Kit	Kapa Biosystems	KK2601
NEBNext® rRNA Depletion Kit (Human/Mouse/Rat)	NEB	E6310L
NEBNext® RNA First Strand Synthesis Module	NEB	E7525S
NEBNext® Ultra Directional RNA Second Strand Synthesis Module	NEB	E7550S
NEBNext® Ultra II DNA Library Prep Kit for Illumina	NEB	E7645S
Deposited Data		
Raw and analyzed data	This paper	GEO: GSE112320
Experimental Models: Organisms/Strains		
Mouse: C57BL/6J$^{flox/flox}$	Tachibana et al., 2007	N/A
Mouse: C57BL/6J$^{flox/flox}$, *Zp3*-Cre	This study	N/A
Oligonucleotides		
Primer: *G9a* flox genotyping forward GCTCCAGGG CGATGGCCTCCGCTGAATGC	Tachibana et al., 2007	N/A
Primer: *G9a* flox genotyping reverse CTGCACG CTGCCTAGATGGAGCATG	Tachibana et al., 2007	N/A
Primer: *G9a* RT-PCR forward CTACCGGACTGCC AAGATGG	This paper	N/A
Primer: *G9a* RT-PCR reverse CTCTGCTCCAGG GCGATG	This paper	N/A
Primer: β-*actin* RT-PCR forward GGCTGTATTCC CCTCCATCG	Lewis et al., 2005	N/A
Primer: β-*actin* RT-PCR reverse CCAGTTGGTAA CAATGCCATGT	Lewis et al., 2005	N/A
Recombinant DNA		
mRNA: EGFP-α-tubulin	Yamagata et al., 2009; Yamagata and Ueda, 2013	N/A
mRNA: H2B-mCherry	Yamagata et al., 2009; Yamagata and Ueda, 2013	N/A
Software and Algorithms		
Bismark v0.14.5	Krueger and Andrews, 2011	https://www.bioinformatics.babraham.ac.uk/projects/bismark/
HISAT2 v2.0.5	Kim et al., 2015	https://ccb.jhu.edu/software/hisat2/index.shtml
StringTie v1.3.3	Pertea et al., 2016	http://www.ccb.jhu.edu/software/stringtie/
bowtie2 v2.2.9	Langmead and Salzberg, 2012	http://bowtie-bio.sourceforge.net/bowtie2/index.shtml
ImageJ 1.51j8	Schneider et al., 2012	https://imagej.nih.gov/ij/

CONTACT FOR REAGENT AND RESOURCE SHARING

Further information and requests for resources and reagents should be directed to and will be fulfilled by the Lead Contact, Hiroyuki Sasaki (hsasaki@bioreg.kyushu-u.ac.jp).

EXPERIMENTAL MODEL AND SUBJECT DETAILS

Animal Work

All animal experiments were performed under the ethical guidelines of Kyushu University, Kindai University, and the Canadian Council on Animal Care. All mice used in this manuscript were euthanized by CO_2 asphyxiation.

Genetically Modified Mice and Genotyping

Mice carrying the flox allele of *G9a* and those carrying the *Zp3-Cre* transgene were described previously (Tachibana et al., 2007; de Vries et al., 2000). Genotyping was performed by PCR using the previously described primers for the *G9a* alleles (Tachibana et al., 2007) and GCAGAACCTGAAGATGTTCGCGAT and AGGTATCTCTGACCAGAGTCATCC for the *Zp3-Cre* transgene. JF1 mice were described previously (Takada et al., 2013).

METHOD DETAILS

Fertility Testing

Female mice of 10 weeks or older were placed together with males in the same cage. Vaginal plugs were checked the next morning. Males were removed after a plug was observed and females were maintained for 20 days. Females that bore live pups were considered fertile. Litter mortality rate refers to the proportion of litters with no pups surviving beyond weaning.

Oocyte Collection, IVF and Embryo Culture

GOs were harvested by sequential digestion of P10 ovaries in 1 mg/ml collagenase (034-10533, Wako Pure Chemical), 0.25% trypsin-EDTA (35555-54, Nacalai Tesque), and 0.5% protease type XIV (P5147, Sigma-Aldrich). FGOs were harvested from P15 or adult (10 weeks or older) ovaries by needle puncture. Superovulation was induced by injecting females sequentially with pregnant mare serum gonadotrophin and human chorionic gonadotropin. Cumulus-oocyte complexes were collected from the oviducts and fertilized with C57BL/6J or JF1 sperm for assessment of preimplantation development, WGBS, and RNA-seq. MII oocytes were harvested by digestion in hyaluronidase (H4272, Sigma-Aldrich). Cumulus cells were removed by capillary washing in PBS and zygotes were cultured in EmbryoMax KSOM Medium (1X) w/ 1/2 Amino Acids (Merck Millipore) or $KSOM^{AA}$ (Ho et al., 1995) at 37°C and 5% CO_2. Two-cell embryos were harvested within 2 hours after the completion of the first mitotic division for WGBS and at 24 hours for RNA-seq. Polar bodies of MII oocytes and 2-cell embryos were removed for WGBS. Blastocysts were harvested at 120 hours for WGBS.

RT-PCR

Total RNA was extracted from pooled oocytes using Trizol reagent (Thermo Fisher Scientific). cDNA was synthesized using PrimeScript RT reagent Kit with gDNA Eraser (Perfect Real Time) (Takara Bio Inc.) and subjected to PCR using KAPA HiFi HotStart ReadyMix PCR Kit (Kapa Biosystems) and TaKaRa PCR Thermal Cycler Dice® (Takara Bio Inc.). PCR primers were: *G9a*, CTACCG GACTGCCAAGATGG and CTCTGCTCCAGGGCGATG; *Actb*, GGCTGTATTCCCCTCCATCG and CCAGTTGGTAACAATGCCATGT.

Western Blotting

Total protein was extracted from pooled oocytes and denatured in a sample buffer (50 mM Tris-Cl, 2% SDS, 0.004% bromophenol blue, and 6% glycerol, pH 6.8) at 85°C for 10 min. Proteins were separated on a 12%–15% SDS-polyacrylamide gel and transferred to a polyvinylidene difluoride membrane by wet blotting. The blot was blocked by 5% skimmed milk or 5% BSA in TBS with Tween-20. Primary antibodies against G9a (ab185050, abcam), H3K9me2 (ab1220, abcam), and β-actin (sc-69879, Santa Cruz) were used. HRP-conjugated IgG (Santa Cruz) was used as the secondary antibody. Signals were detected using Chemi-Lumi One Ultra (Nacalai Tesque) on ImageQuant LAS4000 mini (GE Healthcare Life Sciences). Can Get Signal Immunoreaction Enhancer Solution (TOYOBO) was used to detect H3K9me2.

Ovary Sectioning and Hematoxylin-Eosin Staining

Ovaries were embedded in OCT and flash frozen. Frozen sections were prepared using CM3050 S Research Cryostat (Leica). Hematoxylin-eosin staining was performed under standard procedures.

Immunostaining

Oocytes and embryos were fixed in 2% paraformaldehyde/PBS at room temperature for 30 min. Permeabilization and blocking was performed in 5% BSA and 2% Triton X-100 in PBS for 30 min. Primary antibodies against H3K9me1 (MABI0306, MBL), H3K9me2

(MABI0307, MBL; ab1220, abcam; 39239, Active motif), H3K9me3 (MABI0318, MBL), CDX2 (ab157524, abcam), SOX2 (ab92494, abcam), SOX17 (AF1924, R&D Systems), and HP1β (70-223, BioAcademia) were used. Alexa Flour 488-, 555-, or 647-conjugated IgG (Thermo Fisher Scientific) was used as the secondary antibody. Oocytes and embryos were mounted in VECTASHEILD medium with DAPI (Vector Laboratory) and observed under LSM700 confocal laser scanning microscope (Carl Zeiss). The different anti-H3K9me2 antibodies displayed similar results. Signal intensity was measured using ImageJ 1.51j8 (Schneider et al., 2012).

WGBS, RNA-seq, and ChIP-seq

WGBS libraries were constructed using the post-bisulfite adaptor tagging method (Miura et al., 2012). Pooled oocytes and embryos were spiked with 1% unmethylated lambda phage DNA (Promega). Libraries were amplified with KAPA library amplification kit (KK2620, KAPA) for 4 cycles. For RNA-seq, total RNA was extracted from pooled oocytes and embryos using Trizol reagent (Thermo Fisher Scientific). Libraries were constructed using NEBNext® rRNA Depletion Kit, RNA First Strand Synthesis Module, Ultra Directional RNA Second Strand Synthesis Module, and Ultra II DNA Library Prep Kit for Illumina (NEB). Ultra-low-input native ChIP-seq libraries were prepared from pooled oocytes (Brind'Amour et al., 2015). Zona pellucida was removed by acid Tyrode's solution. ChIP was performed with anti-H3K9me2 antibody (abcam ab1220) in 200 μL NChIP buffer. WGBS libraries were sequenced on HiSeq 1500 or HiSeq 2500 (Illumina) (FGOs and blastocysts: HCS v2.0.5 and RTA v1.17.20; MII oocytes and 2-cell embryos: HCS v2.2.68 and RTA v1.18.66.3) (Toh et al., 2017) using TruSeq SBS kit v3-HS and HiSeq Rapid SBS Kit v2 (Illumina). For RNA-seq and ultra-low-input native ChIP-seq, libraries were sequenced on NextSeq 500, HiSeq 1500, or HiSeq 2500 (Illumina).

Microinjection and Live-cell Imaging

Zygotes were injected with 5 ng/μl mRNAs encoding EGFP-α-tubulin and H2B-mCherry at 5 hours post fertilization (Yamagata et al., 2009; Yamagata and Ueda, 2013). Live-cell imaging was performed on CV-1000 (Yokogawa Electric Corp) from 7.5 to 102 hours at 10-min intervals. Raw images were stacked and projected by CV1000 Software (Molecular Devices) to generate reconstructed movies.

QUANTIFICATION AND STATISTICAL ANALYSIS

Reference Sequences

RefSeq transcript coordinates (RefFlat) and assemblies (GTF) of mouse genome mm10 were obtained from iGenomes (Illumina). Consensus sequences of ERVs (v21.09) were downloaded from Repbase (Bao et al., 2015). The repeat masker track of mm10 was downloaded from UCSC Table Browser (Karolchik et al., 2014). The ICR coordinates (Tomizawa et al., 2011) were adapted for mm10. LAD coordinates were obtained as described (Meuleman et al., 2013).

WGBS Data Analysis

Reads were trimmed to remove low quality bases and adaptor sequences using Trim-Galore! v0.3.3 (Babraham Institute) and mapped to mouse genome mm10 using Bismark v0.14.5 (Krueger and Andrews, 2011). Methylation data at CG (or non-CG) sites covered with 3-100 reads were extracted for the downstream analyses. Windows with less than 5 informative CG (or non-CG) sites were excluded. To study CG methylation at ERVs, reads were mapped to the Repbase annotations. For allelic-specific analysis, reads were mapped to N-masked mm10 genome using published SNP data of JF1 (Takada et al., 2013). Allelic reads were selected using SNPsplit v0.3.2 (Babraham Institute). The methylation data from the ICM (Wang et al., 2014), ESCs (Habibi et al., 2013), liver, and brain (Hon et al., 2013) were reprocessed as above.

RNA-seq Data Analysis

Reads were trimmed and mapped to mouse genome mm10 by HISAT2 v2.0.5 (Kim et al., 2015). Transcripts were assembled by StringTie v1.3.3 (Pertea et al., 2015). Repeat masker-annotated microRNA, rRNA, tRNA-like, and snRNA, and transcripts with a CDS < 200 bp were excluded in the downstream analyses. Genes with (1) FPKM $\geq$ 1, (2) absolute FPKM difference $\geq$ 5, and (3) at least 2-fold changes in all replicates were defined as DEGs. Expression of ERVs was determined using VisRseq (Younesy et al., 2015). ERVs with $\geq$ 100 copies in the genome and at least 2-fold increase in all replicates were defined as derepressed. RefSeq transcripts containing an extra ERV sequence at their 5′ ends were identified as additional chimeric transcripts. For allelic-specific analysis, reads were mapped to N-masked mm10 genome using published SNP data of JF1 (Takada et al., 2013). Allelic reads were selected using SNPsplit v0.3.2 (Babraham Institute). Allelic ratios were determined using at least 20 SNP-containing reads.

ChIP-seq Data Analysis

Reads were trimmed and mapped to mouse genome mm10 by bowtie2 v2.2.9 (Langmead and Salzberg, 2012). Duplicate and low quality reads (MapQ < 5) were removed using Picard v2.6.0 (Broad Institute). Ten-kb windows with H3K9me2 enrichment $\geq$ 1 (i.e., more enriched than input) were identified as H3K9me2-enriched windows. Contiguous H3K9me2-enriched windows were combined and, if they were 20 kb or larger and had overall enrichment $\geq$ 1.22 (third quartile of H3K9me2 enrichment in 10-kb windows), defined as H3K9me2-enriched domains.

Hi-C Data Analysis

A/B compartments were assigned using HOMER v4.9 (Heinz et al., 2010).

Statistical Analysis and Graph Generation

Statistical analyses and graph generation were performed by R v3.2.5 and Excel 2016.

DATA AND SOFTWARE AVAILABILITY

The sequence datasets supporting the results of this article are available in NCBI's Gene Expression Omnibus under accession number GSE112320.